Attitude Motion Characterization of Resident Space Objects via Fusion of Ground-based and Space-based Light Curves

Pasquale Bencivenga, Giorgio Isoletta,
Roberto Opromolla, Giancarmine Fasano
Department of Industrial Engineering
University of Naples "Federico II",
Naples, Italy
pasquale.bencivenga@unina.it,
giorgio.isoletta@unina.it,
roberto.opromolla@unina.it,
g.fasano@unina.it

Abstract— Due to the growing number of fragmentation-related debris and the launch of mega constellations of satellites, the characterization of Resident Space Objects has been assuming a growing importance in the context of Space Situational Awareness programs to enable accurate orbit propagations and related functionalities such as collision avoidance. Based on the analysis of light curves, photometric characterization can provide useful information concerning the objects' surface material, shape, and attitude motion. In this context, this paper proposes an attitude motion classifier of unknown space objects using light curves. In particular, the focus is the combination of data from multiple sensors, either ground or space-based, in order to get a more reliable classification than the one arising from a single photometric measurement. Each light curve is classified using a spectral analysis method based on the Lomb-Scargle Periodogram and the Phase Dispersion Minimization approaches. The classifier's outputs are then fused first at sensor level and then across multiple sensors to derive a unique classification for the observed space object. The performance of the presented architecture is assessed in a numerical environment able to reproduce synthetic light curves accounting for complex object geometries, and a realistic evolution of orbital and rotational dynamics. A correct classification has been produced for all the considered test cases preliminary proving the effectiveness of the proposed approach.

Keywords—Space Situational Awareness, Attitude Motion Characterization, Light Curves, Measurement Fusion, Spectral analysis

I. INTRODUCTION

The last years have shown a notable increase of interest in Space Situational Awareness (SSA), which focuses on gathering and upholding comprehensive knowledge about all objects in Earth's orbit. Resident Space Objects (RSOs), namely, artificial objects destined to orbit for an extended time period, play a crucial role in human life (providing essential functions in the fields of communication, navigation, Earth observation, scientific research and defense), and represent one of the major interests of SSA programs. The consistent number [1] of inactive RSOs poses a serious problem to space traffic management due to the risk of collisions between two or more objects. Indeed, these events can compromise the activities of operative satellites by boosting the increase in debris population.

One of the main segment of SSA is Space Surveillance & Tracking (SST). The characterization of RSOs through photometric measurements, i.e., light curves (LCs), is a fundamental task in this context since it allows to obtain information about different properties of the target such as its attitude motion, shape, dimension, and composition. Indeed, a light curve, defined as the time trend of an object's brightness observed by an optical sensor, is not solely influenced by the Sun-object-sensor observation geometry, but also by the object's shape, its surface materials' composition and roughness, and its rotational dynamics. The analysis of light curves is essential for numerous space surveillance and debris management tasks, yet it can be hindered by noise problems, primarily arising from light interference from other objects, atmospheric conditions, and optical sensor constraints.

The process of recovering an object's inherent characteristics from collected brightness variations over time is known as light curve inversion. This operation is not trivial due to the intricate relationship between the object's properties, the observation geometry, and the noise sources. As a consequence, most literature works focus on the estimation of some parameters concurring to the light curve formation while assuming the others are known. For instance, the rotational dynamics can be inferred from the light curve if shape and surface properties of the observed object are known [2].

Light curve inversion methods can generally be divided in three main classes: (*i*) frequency-based approaches, i.e., relying on a spectral analysis of the light curve brightness signal; (*ii*) filtering techniques, i.e., relying on a recursive filter; (*iii*), data-driven approaches, i.e., relying on Machine Learning (ML) based algorithms [3]. The work by Linder et al. [4], which provides an overview about methods to perform the analysis of light curves, also distinguishes between the possibility to rely on evenly and unevenly temporally spaced data. Concerning spectral analysis methods, the works by Isoletta et al. [5] and Quint et al. [6] implement the Lomb-Scargle Periodogram (LSP). The former work addresses the classification of the attitude motion among three categories (i.e., "Tumbling", "Spin stabilized" and "Uncertain") and support the classification made by the LSP by means of the Phase Dispersion Minimization (PDM); the latter deals with

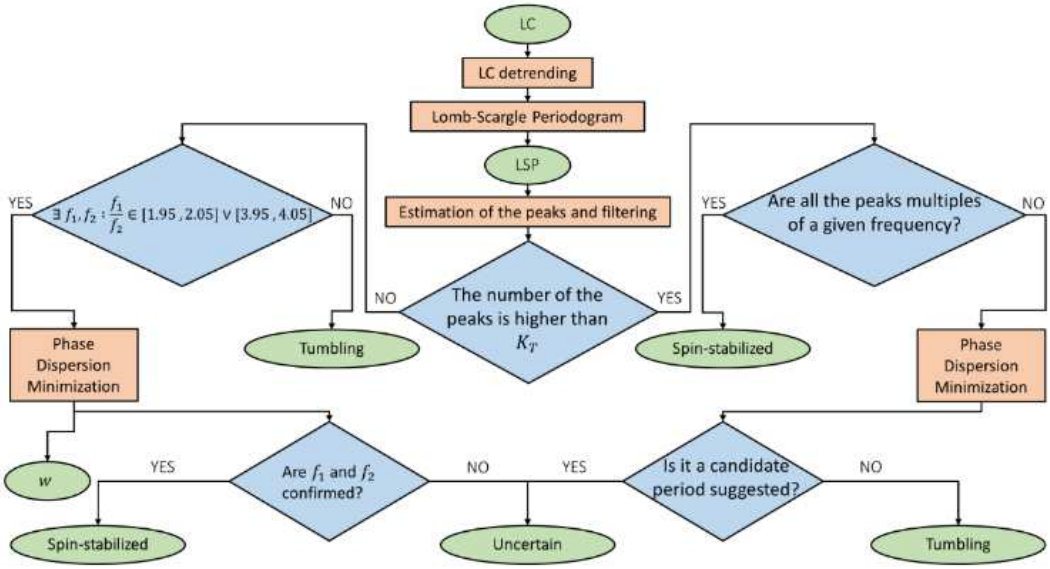

Fig. 1. Workflow of the single LC classifier

the fusion of multiple types of measurements, such as photometric and laser measurements, to estimate the apparent rotation period of a space object. Wetterer and Jah [7] alternatively propose an Unscented Kalman Filter to estimate the attitude and the angular velocity of objects in LEO, assuming known surface properties and shape. Other approaches in this class make use of a Particle Filter, such as the work by Linares et al. [8], in which the estimated attitude is parametrized using the Generalized Rodrigues Parameters. Regarding the third class, ML-based algorithms show a noticeable adaptability to the context of RSOs characterization, since they are used with a good accuracy in several tasks including the estimation of the shape [9] and the attitude reconstruction [10]. Finally, photometric data can also be integrated with astrometric measurements, as proposed by Linares et al. in [11], where an estimation of the mass and area of RSOs is made assuming the knowledge of its shape.

Building upon the work in [5], this paper aims to contribute to the literature on light curve inversion methods based on spectral analysis. Specifically, it proposes an original architecture, entirely developed in MATLAB, to fuse light curve measurements from multiple ground- and space-based sensors thus adding spatial and temporal diversity of photometric measurements to the previous work in order to obtain additional information and improve the attitude motion classification accuracy of RSOs. In particular, the objective of this work is to assess a classification to a space object's attitude motion in one of three categories: "Spin-Stabilized", "Tumbling", and "Uncertain". The remainder of the paper is organized as follows. Section II presents the methodology used to analyze the light curves coming from different sources and to merge them to obtain the attitude motion classification. Section III briefly describes the simulation environment conceived to generate synthetic light curves from multi-spatial information sources. Section IV presents and discusses the classification results for a simulated test case. Finally, conclusions are drawn in Section V.

II. Methodology

Measurement and sensor fusion can enhance the accuracy, reliability, and richness of the data by combining information from different sources. In this work, the fusion task refers to the combination of photometric measurements generated by multiple ground- and space-based sensors by means of a combined LC-based classifier. Indeed, the variability in the number and characteristics of the sensors grants different observation perspectives on the orbiting target, which may result in increased visibility and, in general, quality of acquired data. In addition, in Low Earth Orbits, the problem of short exposure times of a target observed by a ground-based sensor, representing a key challenge to the light curve inversion process, can be addressed considering the fusion of photometric measurements obtained by space-based sensors. This section is organized as follows. The single-LC classifier is recalled in *Sub-section A*; *Sub-section B* describes the logic behind the measurement fusion applied for merging the several LCs acquired by a single sensor; finally, *Sub-section C* explains the combination procedure to get a final classification from the statuses in output from all the ground- and space-based sensors. The following notation is adopted: the *j*-th LC of the *i*-th sensor is identified as LC_j^i. If the number of ground sensors is *N* and the number of space sensors is *M*, then *i* goes from 1 to $(N + M)$. Considering that the *i*-th sensor produces K_{LC}^i light curves, *j* can vary from 1 to K_{LC}^i.

A. Single LC classifier

Since photometric measurements are not regularly sampled in time, one of the most effective techniques to recover the frequency spectrum of light curves is the Lomb-Scargle Periodogram, analyzed in detail by Van der Plas in [12], where it is described as a method that allows efficient computation of a Fourier-like power spectrum from unevenly-sampled data, resulting in an intuitive means of determining the period of oscillation. To assist the selection of a single oscillation period between those retrieved by LSP, this technique is often coupled with the PDM [13], which is particularly effective when only a few observations are available over a limited time period, most notably when the light curve is far from a sinusoidal behavior in time, PDM

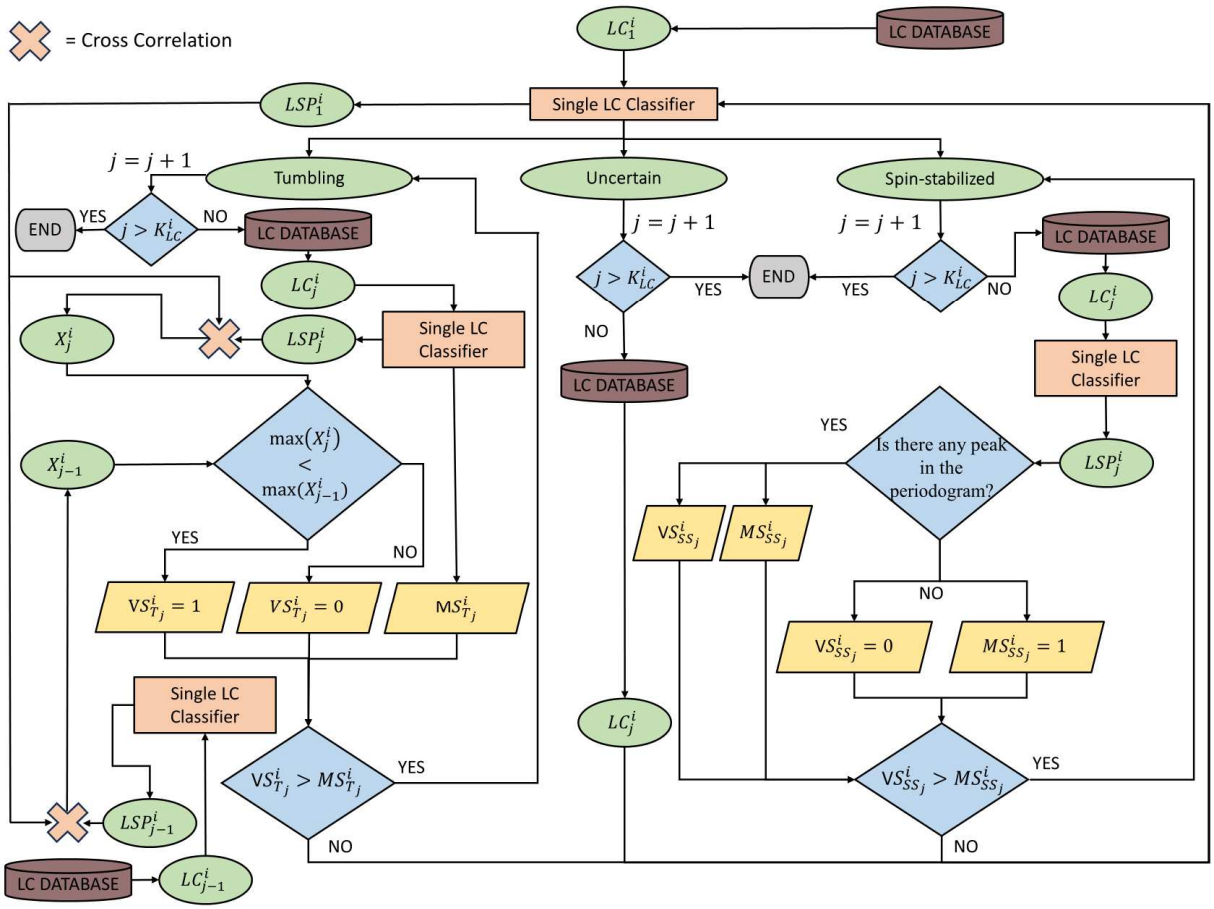

Fig. 2. Workflow of the multiple LC classifier

has the objective to minimize the variance of the data with respect to the light curve's mean and consists of a formula that attributes a score to the operation of data folding by a candidate period (which can be chosen among the ones given by the LSP), providing a means to compare such periods.

The classification method presented in [5] relies both on LSP and PDM. The operative conditions that drive to a classification rather than the others are shown in the workflow represented in Fig. 1 which represents the logic of the single light curve classifier. The whole workflow is based on the processing of the LSP's peaks which are found analyzing two characteristics: their value and their prominence. In particular, a first condition to satisfy is that the power value under investigation must be greater than the maximum value of the complete LSP divided by a user-defined factor, which has been set equal to 15 in this work. Meanwhile, prominence refers to the relative height or significance of a power value showing how much higher it is compared to the surrounding noise level. A "prominent" value means that it is more likely to be significant and not just a result of random fluctuations in the data. Thus, the peaks that have met the first condition are discarded if their prominence is lower than the maximum prominence value in the LSP divided by a user-defined factor, which has been set equal to 20 in this work [5]. K_T is a user-defined threshold on the number of retrieved peaks, while f_1 and f_2 are peak frequencies of the LSP. K_T has been empirically set to 7, since the periodograms retrieved from the light curves of tumbling objects often have a higher number of peaks with respect to those of stabilized objects[5]. It is important to highlight that the single LC classifier outputs the LSP, the resulting attitude classification and an estimate of the associated angular velocity w.

B. *Multiple LC classifier*

If more than one LC is collected by a single sensor, the architecture described in the previous section will provide multiple estimates of the object attitude status not necessarily consistent with each other: so, an information fusion is needed to derive a single classification. This task is accomplished by a multiple LC classifier whose workflow is depicted in Fig. 2. All the available LCs are first arranged in a chronological order, and the first one is passed to the single LC classifier. Based on the resulting estimated status a different processing pipeline is then followed. If the classification is "Uncertain", the tool proceeds by analyzing the subsequent LCs (i.e., increasing j) until a different classification is obtained; if this does not occur, the final classification assigned to the object by the i-th sensor is "Uncertain". As soon as one LC is classified as Tumbling or Spin Stabilized, the tool tries to confirm such result. Thus, the next LC is analyzed in a distinct way with respect to the classification made only by the single LC classifier through the attribution of a couple of scores indicated as Miss Score (MS) and Validate score (VS), computed as detailed in the following.

If a "Spin-stabilized" classification occurs, the successive LC is processed applying the LSP algorithm. If no peak is found in the periodogram, the Spin-stabilized Validate Score ($VS_{SS_j}^i$) and the Spin-stabilized Miss Score ($MS_{SS_j}^i$) are set equal to 0 and 1, respectively, and the LC is processed again

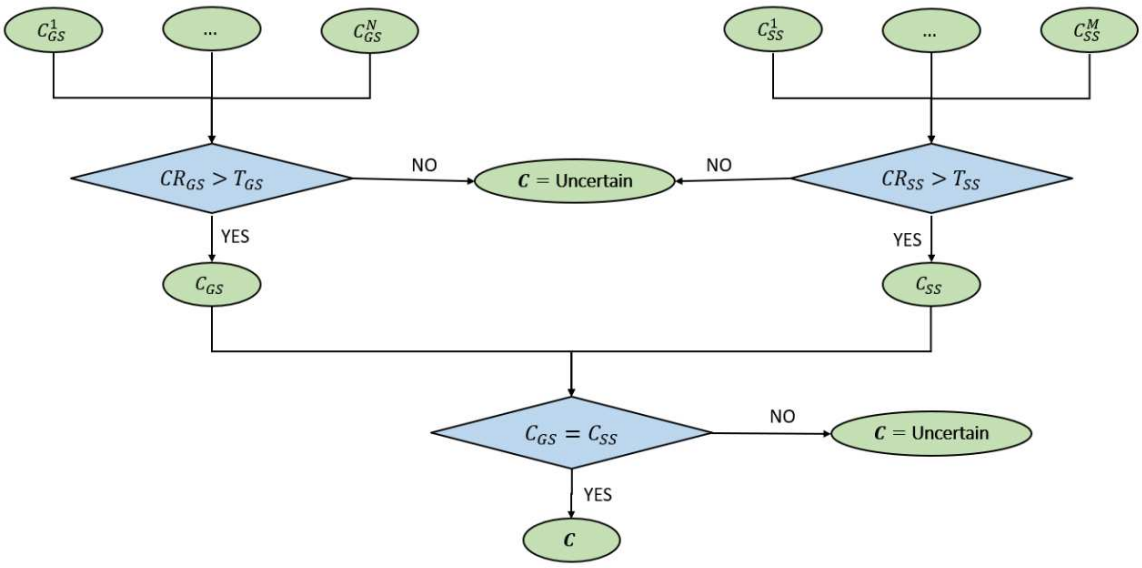

Fig. 3. Workflow of the sensor combination process

by the single LC classifier following the pipeline in Fig. 2. Instead, the tool looks for the maximum power value ($P^i_{CS_{MAX_j}}$) within a frequency interval defined around f^i_{j-1}, computed as shown in (1).

$$f^i_{j-1} = 2 \cdot \frac{w^i_{j-1}}{2\pi} \tag{1}$$

The above-mentioned frequency interval is defined as $\left[\frac{f^i_{j-1}}{1+\Delta t f^i_{j-1}}, \frac{f^i_{j-1}}{1-\Delta t f^i_{j-1}}\right]$, where Δt is set to 1 s, which allows to consider frequencies corresponding to rotation periods very close to the one estimated for the (j-1)-th light curve.
Therefore, by defining $P^i_{LS_{MAX_j}}$ as the overall maximum power value of the LSP, $VS^i_{SS_j}$ and $MS^i_{SS_j}$ are calculated as shown in (2) and (3).

$$VS^i_{SS_j} = \frac{P^i_{CS_{MAX_j}}}{P^i_{LS_{MAX_j}}} \tag{2}$$

$$MS^i_{SS_j} = 1 - VS^i_{SS_j} \tag{3}$$

At the end of this process, if $VS^i_{SS_j} > MS^i_{SS_j}$ then the current j-th light curve is classified as Spin-stabilized and the subsequent LC is processed with the same logic. Otherwise, the classification of the j-th LC is given by the single LC classifier and the analysis of the successive light curve is done depending on such classification.
From the workflow in Fig. 2 it is evident that the couple of scores is not always calculated. So, it is important to point out that if it is not possible to compute VS and MS for certain light curves because of the "Uncertain" status or because they enter in a "classification loop" for the first time, they are both set equal to zero for that LC.

If a "Tumbling" classification is retrieved following the pipeline in Fig. 2, the subsequent LC is processed to try confirming this classification. When an object is in a tumbling state, the periodograms corresponding to LCs subsequent in time tend to be less similar. This phenomenon is quantified by a decreasing trend of the maximum cross-correlation between the two LC [14]. Thus, by indicating as X^i_j and X^i_{j-1} the cross correlations between the LSP of the first LC and those of the LCs of the current and previous steps, respectively, it must be verified that the maximum value of X^i_j is less than or equal to the maximum value of X^i_{j-1}. If this condition is met, then a Tumbling Validate Score ($VS^i_{T_j}$) is set to 1, otherwise it is set to 0. By contrast, the value of the Tumbling Miss Score ($MS^i_{T_j}$) depends on the result of the single LC classifier, meaning that if the output is a "Tumbling" status, the score is imposed to be equal to 0, otherwise it is set to 1.

Similarly to the Spin-Stabilized case, if $VS^i_{T_j}$ is greater than the $MS^i_{T_j}$, then the current LC is classified as Tumbling and the process continues. Otherwise, the LC is processed again by the single LC classifier following the pipeline in Fig. 2.

The entire process ends when there are no more light curves available for the sensor.
To assess the final classification for the sensor, a final score that takes into account all the VSs assigned is calculated. A weight is associated to each light curve, and it is multiplied by the related VS to determine the status in output from a sensor.
The weights are introduced to consider the fact that some LCs may be more valuable than others, since they may last longer or have denser data. In details, the weight W^i_j is calculated as:

$$W^i_j = \frac{K^i_{m_j}}{K^i_{s_j}} \cdot \frac{D^i_j}{AD^i} \tag{4}$$

$K_{s_j}^i$ is the number of time samples during the observation window for the acquisition of the *j*-th LC, while $K_{m_j}^i$ is the number of measurements acquired by the *i*-th sensor during the observation, i.e., the time instants in which the apparent visual magnitude is different from 0. D_j^i is the duration of the light curve under consideration, while AD^i is the average duration of the observation windows collected by the *i*-th sensor.

When all the LCs of a sensor have been processed, then a final score for the Spin-stabilized case, FS_{SS}, and Tumbling case, FS_T, are calculated to confirm such status as shown in (5) and (6).

$$FS_{SS}^i = \sum_j^{K_{LC}^i} \left(VS_{SS_j}^i \cdot W_j^i \right) \tag{5}$$

$$FS_T^i = \sum_j^{K_{LC}^i} \left(VS_{T_j}^i \cdot W_j^i \right) \tag{6}$$

Afterwards, the values of the final scores are compared to the most frequent classification, i.e., the classification that occurs the most during the processing of the *i*-th sensor. Indeed, if such classification is "Spin-stabilized" and $FS_{SS}^i > FS_T^i$ then the status is confirmed, otherwise the classification of the sensor is assessed as "Uncertain". The same procedure is done for the "Tumbling" case implying that if $FS_T^i > FS_{SS}^i$ then the status is confirmed, else it is classified as "Uncertain". If the most frequent classification is "Uncertain", no comparison is made since the tool classifies the sensor as "Uncertain" directly.

C. Sensor combination

A further step in the information fusion consists in the combination of the classification outputs of all the sensors belonging to the same category, i.e., ground- or space-based sensors. This procedure, whose workflow is depicted in Fig. 3, is done by selecting a user-defined threshold for the cluster of ground-based sensors, T_{GS}, and another one for the group of space-based sensors, T_{SS}, both ranging from 0 to 1.In particular, it is advised to use values of T_{GS} and , T_{SS} equal to 1 if the number of ground-based and space-based sensors, respectively, is less than 4. With the increasing number of sensors, the thresholds can be lowered since each sensor becomes less important within its category. Thus, by considering the classifications of the ground-based sensors (C_{GS}^1, … , C_{GS}^N) and the ones of the space-based sensors (C_{SS}^1, … , C_{SS}^M), the most common classification for the ground sensors C_{GS} and space sensors C_{SS} is considered. Two ratios are defined by dividing the number of the occurrences of C_{GS} and C_{SS} by *N* and *M* respectively, obtaining the "Classification Ratio" values, denoted as CR_{GS} and CR_{SS} for the ground-based and space-based sensors. If the value of CR_{GS} is greater than T_{GS}, then the target's classification by the ground-based sensors is confirmed to be C_{GS}, else the classification is addressed with the "Uncertain" status. The same logic is applied to the space-based group so that there is the possibility to confirm the status given by C_{SS} or to impose the "Uncertain" status.
Finally, the two outputs of the clusters are merged performing a matching between them: if they are equal then the target is classified with that status, else the status "Uncertain" is assigned to the target. It is worth noting that with this logic, a single "Uncertain" status, given either by the ground-based category or the space-based one, is sufficient to assign "Uncertain" as the final classification.

III. Simulation Environment

The production of synthetic light curves is part of a more extensive simulation environment, which includes a coupled propagator providing both the orbital and attitude propagation of an object of interest over a user-defined simulation time.

The inputs of the tool are the following:

- Geometric model and reflectivity properties of the target: the object can be modeled by importing a CAD of any complexity or as a combination of elementary shapes whose surfaces are then sampled by means of a triangular mesh. Each triangular element is then associated with an area, normal unit vector, and diffusive and specular reflectivity values.
- Initial state vector: the state vector includes the orbital and the attitude states of the target. The target's position and velocity are expressed in the Earth-Centered Inertial (ECI) reference frame, while the angular velocity of the target in the Body Reference Frame (BRF) and the target's quaternion represents the orientation of the BRF with respect to ECI.
- Initial and final epochs of interest for the simulation.
- Set of orbital perturbations to consider: the tool is capable of propagating the target under the effect of gravity, aerodynamic drag, solar radiation pressure and third body disturbance. The perturbation settings may be fully customized, by selecting the degree and order of gravity harmonics, the atmospheric density model between four different models available, and which third bodies to consider (Moon and Sun available).
- Optical sensors' properties (e.g., the Field of View).
- Geodetic coordinates of ground-based sensors.
- Orbital states of space-based sensors.

The outputs of the tool are the following:

- Time history of the state vector of the target.
- Light curves of the target acquired by each sensor and for each observation window.

The last task of the tool i.e., the synthesis of light curves, is made possible thanks to use of the Cook-Torrance model [15] to reproduce the optical behavior of the target. By denoting with the letter $\mathcal{M}$ the visual apparent magnitude of the target under observation, a light curve has been defined as the collection of the variation of $\mathcal{M}$ during the observation window. The equation that models the apparent visual magnitude is shown in (7).

$$\mathcal{M} = -26.7 - 2.5 \cdot \log_{10} \left(\frac{\mathcal{B}}{\mathcal{B}_{SUN}} \right) \tag{7}$$

where the value of -26.7 depicts the apparent magnitude of the Sun, while $\mathcal{B}$ and $\mathcal{B}_{SUN}$, representing irradiances $[\frac{W}{m^2}]$, denote the brightness values of the target and the Sun, respectively.

The computation of these values is made by means of the Cook-Torrance model by involving the contributions of all the illuminated and visible meshed areas of the target. The visibility of a facet is determined by the fulfillment of two conditions at the same time: the facet must be illuminated by the Sun, and it must be in view of the sensor.

IV. Results

This section contains a discussion about the main results obtained with the proposed classification method described in Section II.

The complex nature of the problem implies a high number of possible test cases by changing, for instance, the geometry of the target and its orbital state, the number of ground-based and space-based sensors, their properties, the orbital states of space-based sensors, and the simulation time.

The scenario described in this section depicts the simulation and classification of light curves of a cylinder-shaped object, shown in Fig. 4, also presented in [5], whose extremities are paraboloids in order to emulate the structure of a rocket body. The target is modeled in this way to emulate the behavior of the Atlas Centaur 2 rocket body (NORAD ID: 694).

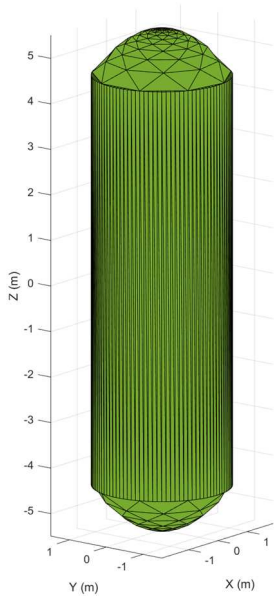

Fig. 4. CAD model of the target

The initial angular velocity w_0 in the BRF is expressed in (8), representing a spin-stabilized attitude motion, while the initial quaternion q_0, considering the last component as the scalar one, is represented in (9).

$$w_0 = [0,1.5,0]\ ^\circ/s \tag{8}$$

$$q_0 = [0,0,0,1] \tag{9}$$

The target is propagated for ten hours starting from the 24th of March 2003 at 13:30:00. The initial orbital state of the target is reported in Table 1, where a is the semimajor axis, e is the eccentricity, RAAN stands for the Right Ascension of the Ascending Node, i is the inclination, and AoP stands for the Argument of Perigee.

Table 1. Initial orbital parameters of the target

a [km]	e	RAAN [°]	i [°]	AoP [°]
7302	0.06	74.1	30.3	327.6

Four ground-based and one space-based sensors have been chosen to perform the simulation. Having this framework, T_{GS} is set equal to 0.75 while T_{SS} is set equal to 1.

The characteristics of the four ground-based sensors are reported in Table 2. The geodetic coordinates, i.e., longitude, latitude, and altitude, are expressed in WGS84. All the telescopes are assumed to be omnidirectional, i.e., they can be pointed to acquire measurements on the objects of interest without being affected by obstructions. The dusk angle is defined as the minimum angle below the local horizon of the sensor at which the Sun must be for an object to be observable, while the mask angle is the minimum elevation angle above the observer's horizon that an object must have in order to be observable. A Signal-to-Noise Ratio (SNR) equal to 20 has been considered as a realistic value [16].

Table 2. Characteristics of the ground-based sensors

	Ground sensor 1	Ground sensor 2	Ground Sensor 3	Ground Sensor 4
Longitude [°]	-156.3	12.4	-16.9	16.8
Latitude [°]	20.7	41.7	32.7	52.6
Altitude [m]	3075.0	81.0	1818.0	58.0
Dusk angle [°]	4	4	4	4
Mask angle [°]	10	10	10	10
SNR	20	20	20	20

The initial orbital state of the space-based sensor is reported in Table 3, while its characteristics are shown in Table 4.

Table 3. Initial orbital parameters of the space-based sensor

a [km]	e	RAAN [°]	i [°]	AoP [°]
6917	0.0009	205.6	53.0	323.9

Table 4. Characteristics of the space-based sensor

FOV [°]	Aperture [cm]	SNR
1.4	15	6.5

All the five sensors achieve the acquisition of photometric measurements, and their observation windows are shown in Table 5. In particular, the appearance of the same sensor in the left column means that such sensor observes the target more than one time.

The light curve acquired by the first ground sensor and the relative LSP are depicted in Fig. 5 and Fig. 6, respectively. In addition, Fig. 7 - Fig. 10 show the LCs and the corresponding LSPs obtained by the second ground sensor and the space sensor during their last observation windows.

Table 5. Observation windows of the sensors

	Initial observation time	***Final observation time***
Ground sensor 1	14: 48: 26	15:02:29
Ground sensor 2	19:30:53	19:39:00
Ground sensor 2	21:17:42	21:30:17
Ground sensor 3	21: 10: 39	21:21:55
Ground sensor 4	21:22:51	21:27:14
Space sensor	14:05:57	14:06:09
Space sensor	14:31:33	15:02:22
Space sensor	16:10:21	16:40:01
Space sensor	17:52:39	18:14:37

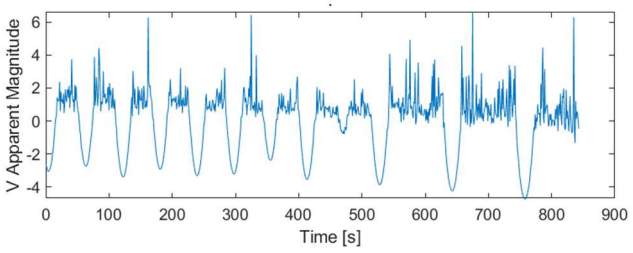

Fig. 5. LC acquired by the first ground-based sensor

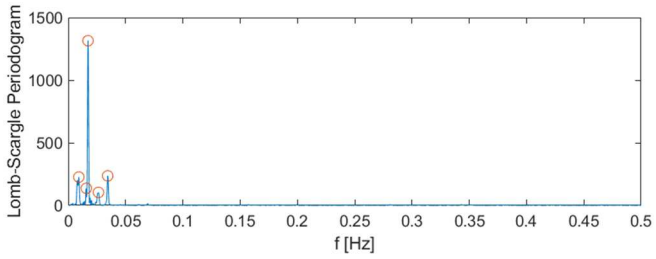

Fig. 6. LSP of the LC acquired by the first ground-based sensor

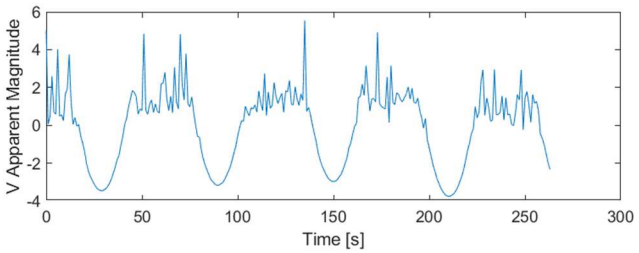

Fig. 7. LC acquired by the fourth ground-based sensor

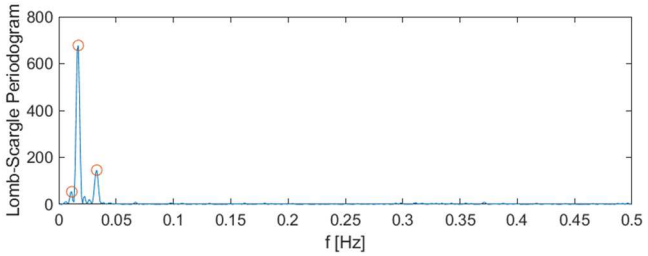

Fig. 8. LSP of the LC acquired by the fourth ground-based sensor

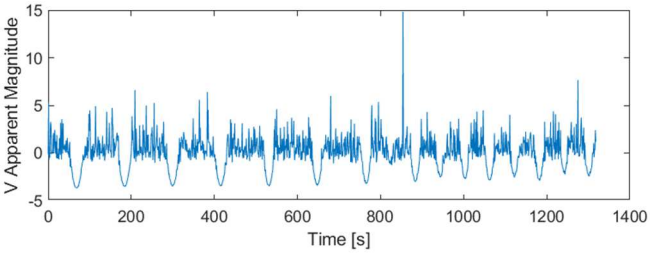

Fig. 9. Last LC acquired by the space-based sensor

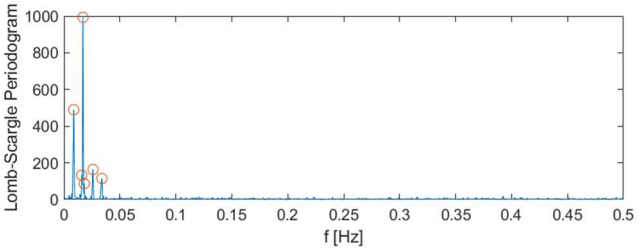

Fig. 10. LSP of the last LC acquired by the space-based sensor

Analyzing in detail the whole process that leads to the final classification, the first ground-based sensor shows a single observation window, implying that its status is assessed by the single LC classifier, which gives in output the "Spin-stabilized" classification. The third ground-based sensor undergoes the same procedure. For the second ground-based sensor, which collects photometric measurements in two different observations windows, the classification is "Spin-stabilized" for both the windows resulting in a null value for FS_T^2, since no "Tumbling" statuses have occurred, while FS_{SS}^2 is equal to 0.6361 implying a "Spin-stabilized" classification for this sensor. The fourth ground-based sensor presents a single observation window, and the collected light curve is classified by the single LC classifier which assigns a "Tumbling" status. The space-based allows to have longer observation windows and gives in output an "Uncertain" status followed by three "Spin-stabilized" classifications according to the chronological sequence of the windows. A null value for FS_T^3 and a value of 1.1040 for FS_{SS}^3 are assigned implying a "Spin-stabilized" status. For the ground-based category, the occurrences of the "Spin-stabilized" status result to be the 75% of the total equaling T_{GS}. Thus, since both ground- and space-based sensors have the same status, the final classification of the target, that combines the ones by the two groups, is the "Spin-stabilized" status which, indeed, represents the truth.

In the synthesis of photometric measurements, the contribution of the noise is modeled as a white gaussian noise whose standard deviation is set equal to the mean of the measurements of brightness obtained by the sensor and divided by the SNR of such sensor. Thus, the noise is added to the brightness measured by the sensor implying that the process is influenced by a random component. To measure the impact of such phenomenon, a sensitivity test has been made by iterating the acquisition of photometric measurements and the consequent classification process one thousand times. The results show that the "Spin-stabilized" status is confirmed by each iteration obtaining a final success rate of 100%.

Furthermore, although they were not included in this paper due to size limits, other test cases in which the target is

simulated with a different behavior were evaluated. In particular, values for the components of the angular velocity lower than 10°/s are chosen in order to emulate the motion of tumbling objects. In these scenarios, the results given by the sensitivity tests show lower success rates (60-80%) with respect to the simulation analyzed in this work. A possible reason may be the cylindrical symmetry of the object which can lead to a periodic pattern of the visual apparent magnitude independently of the object's true attitude.

V. Conclusions

This paper contributes to the ongoing discourse on Space Situational Awareness (SSA) by focusing on one of most important aspects of Space Surveillance & Tracking (SST): the characterization of Resident Space Objects (RSOs). In particular, the core of the work is constituted by the inversion process of light curves to estimate the target's attitude motion by exploiting a multi-sensor fusion framework in which multiple ground-based and space-based sensors are present. A realistic test case with a spin-stabilized target is considered showing the potential of the measurement fusion and sensor combination that allow to improve the accuracy and the reliability of the results with respect to the ones obtained from a single sensor in such scenario.

Tests on real light curves are necessary to obtain further validation of the accuracy and reliability of the developed framework. A possible further development consists in considering the possibility of incorporating additional a priori information about the considered RSO.

Acknowledgment

This work has been developed within the project "Attività tecnico-scientifiche di supporto a C-SSA/ISOC e simulazione di architetture di sensori per SST" funded by the Italian Space Agency (ASI).

References

[1] L. Miraux, "Environmental limits to the space sector's growth," *Science of The Total Environment*, vol. 806, p. 150862, Feb. 2022, doi: 10.1016/J.SCITOTENV.2021.150862.

[2] F. Piergentili, G. Zarcone, L. Parisi, L. Mariani, S. H. Hossein, and F. Santoni, "LEO object's light-curve acquisition system and their inversion for attitude reconstruction," *Aerospace*, vol. 8, no. 1, pp. 1–18, Jan. 2021, doi: 10.3390/aerospace8010004.

[3] S. Jahirabadkar, P. Narsay, S. Pharande, G. Deshpande, and A. Kitture, "Space Objects Classification Techniques : A Survey," in *International Conference on Computational Performance Evaluation (ComPE)*, 2020.

[4] E. Linder, J. Silha, T. Schildknecht, and M. Hager, "Extraction of spin periods of space debris from optical light curves," in *66th International Astronautical Congress*, Curran Associates, Inc., 2015. doi: 10.7892/boris.73954.

[5] G. Isoletta, F. Cuomo, R. Opromolla, and G. Fasano, "Characterization of space objects' attitude motion using Lomb-Scargle Periodogram," 2023, doi: 10.13009/EUCASS2023-754.

[6] G. Quint, A. de Andrés, M. Viturro, J. Carro, V. Morand, and M. Steindorfer, "An Advanced Tool to Determine the Apparent Rotation Period of a Space Object from a Fusion of Measurements," in *73rd International Astronautical Congress*, 2022. [Online]. Available: https://www.eusst.eu/wp-content/uploads/2022/11/IAC-22_rotation_period.pdf

[7] C. J. Wetterer and M. Jah, "Attitude estimation from light curves," *Journal of Guidance, Control, and Dynamics*, vol. 32, no. 5, pp. 1648–1651, 2009, doi: 10.2514/1.44254.

[8] R. Linares, J. Crassidis, and M. Jah, "Particle filtering light curve based attitude estimation for non-resolved space objects," 2016. [Online]. Available: https://www.researchgate.net/publication/287186791

[9] M. Howard, B. Klem, and J. Gorman, "RSO Characterization with Photometric Data Using Machine Learning."

[10] A. B. Burton, C. Frueh, and L. Robinson, "Attitude Estimation using Light Curves: A Particle Swarm Approach," in *AIAA SCITECH 2024 Forum*, Reston, Virginia: American Institute of Aeronautics and Astronautics, Jan. 2024. doi: 10.2514/6.2024-0199.

[11] R. Linares, M. Jah, and J. Crassidis, "Inactive space object shape estimation via astrometric and photometric data fusion." [Online]. Available: https://www.researchgate.net/publication/287186964

[12] J. T. VanderPlas, "Understanding the Lomb-Scargle Periodogram," Mar. 2017, doi: 10.3847/1538-4365/aab766.

[13] R. F. Stellingwerf, "Period Determination Using Phase Dispersion Minimization," *Astrophys J*, vol. 224, pp. 953–960, 1978, doi: 10.1086/156444.

[14] M. D. Abercrombie, B. Calef, and S. Naderi, "Light Curve Analysis of Deep Space Objects in Complex Rotation States," AMOS, 2021. [Online]. Available: www.amostech.com

[15] R. L. Cook and K. E. Torrance, "A Reflectance Graphics Model for Computer," *ACM Trans Graph*, vol. 1, no. 1, pp. 7–24, Jan. 1982, doi: 10.1145/357290.357293.

[16] S. Fan and C. Frueh, "A Direct Light Curve Inversion Scheme in the Presence of Measurement Noise," *Journal of the Astronautical Sciences*, vol. 67, no. 2, pp. 740–761, Jun. 2020, doi: 10.1007/s40295-019-00190-3.